DFT and ab Initio Dual-Level Direct Dynamics Studies on the Reactions of Fluorine Atom with HOCl and HOBr

Li Wang, Jing-yao Liu, Ze-sheng Li,* and Chia-chung Sun

Institute of Theoretical Chemistry, State Key Laboratory of Theoretical and Computational Chemistry, Jilin University, Changchun 130023, P. R. China

Received: February 22, 2005; In Final Form: June 21, 2005

The multichannel reactions (1) HOCl + F → products and (2) HOBr + F → products have been investigated using the dual-level direct dynamics method. The minimum energy paths (MEPs) are calculated at both the MPW1K/6-311G(d,p) and QCISD/6-311G(d,p) levels, then the single-point energies are further corrected at the QCISD(T)/6-311++G(3df,3pd) level of theory. There are hydrogen-bonded complexes with the energies less than those of the reactants or products located at the entrance or exit channel of both hydrogen abstraction reactions; while for the halogen abstraction channels only one complex exists at the reactant side in the bromine abstraction channel. The rate constants are evaluated by the improved canonical variational transition-state theory (ICVT). The agreement of the rate constants with available experimental values for two reactions at room temperature is good. Theoretical results indicate that for the reaction HOCl + F, hydrogen abstraction channel leading to the formation of HF + ClO will predominate the reaction over the whole temperature range, and the reaction of HOBr + F may proceed mainly through the bromine abstraction channel at the lower temperature while the contribution of hydrogen abstraction channel will become significant as the temperature increases. Because of lack of the kinetic data of these reactions, the present theoretical results are expected to be useful and reasonable to estimate the dynamical properties of these reactions over a wide temperature range where no experimental value is available.

Introduction

Hypohalous acids (HOCl and HOBr) are known to be an important atmospheric reservoir for ClO_x and BrO_x, and thus they act as intermediates promoting ozone depletion in the polar stratosphere.[1−4] Photolysis appears to be the principal means of their destruction in the stratosphere, while the reactions of HOCl and HOBr with atmospheric radical species also attract attention in kinetic modeling study. Vogt and Schindler[5] studied the kinetics of the reaction HOCl with F atom:

$$F + HOCl \rightarrow HF + ClO \quad (R1a)$$

$$\rightarrow ClF + OH \quad (R1b)$$

The total rate constants were determined at room temperature. On the basis of their study they concluded that the hydrogen abstraction channel is the major channel with the ratio of $k_{1a}/k_1 = 0.76 \pm 0.09$. For the reaction of F atom with HOBr:

$$F + HOBr \rightarrow HF + BrO \quad (R2a)$$

$$\rightarrow BrF + OH \quad (R2b)$$

Mooks et al.[6] reported the total rate constant of $(2.0 \pm 0.7) \times 10^{-11}$ cm^3 molecule^{-1} s^{-1} at 298 K; however, the branching ratios were not given in the literature. Moreover, no Arrhenius expression was reported for both reactions. Recently we have investigated the mechanisms of the analogous reactions of HOCl with Cl and H atoms.[7] The calculations show that these two reactions proceed practically via Cl-abstraction. Thus, the questions arise: which is the major abstraction channel for the HOCl + F and HOBr + F reactions? Are the reaction mechanisms of R1 and R2 similar to those of the HOCl + Cl and HOCl + H reactions? To gain a deep insight into the mechanisms of the above two reactions (R1 and R2), further theoretical studies are very desirable. To the best of our knowledge, little theoretical attention has been paid to the reactions of F atoms with HOCl and HOBr.

Here, a dual-level approach (X//Y)[8−10] is employed to study the kinetic nature of the reactions. In this methodology, information on the potential energy surface (PES) is obtained directly from ab initio or density functional theory (DFT) electronic structure calculations. Subsequently, by means of the Polyrate 8.4.1 program,[11] the rate constants are calculated using the variational transition-state theory (VTST)[12−14] proposed by Truhlar and co-workers. The comparison between theoretical and experimental results is discussed.

Calculation Methods

The electronic structure calculations are carried out using the Gaussian 98[15] program. The geometries and frequencies of all the stationary points, including reactants, complexes, transition states (TSs), and products involved in two reactions, are optimized at two levels, namely modified Perdew−Wang 1-parameter model for kinetics (MPW1K) and quadratic configuration interaction with single and double substitutions (QCISD) levels with the 6-311G(d,p) basis set (i.e., MPW1K/6-311G(d,p) and QCISD/6-311G(d,p)). The minimum-energy path (MEP) is calculated by the intrinsic reaction coordinate (IRC) theory at above two levels to confirm that the TS really connects with minima along the reaction path. To yield more reliable reaction energies and barrier heights, single-point

* Corresponding author. Fax: +86-431-8498026. E-mail: ljy121@mail.jlu.edu.cn; liujy121@163.com.

10.1021/jp050916y CCC: $30.25
Published on Web 09/16/2005

calculations for the stationary points are carried out at the quadratic configuration interaction with single and double substitutions and perturbative inclusion of connected triple substitutions with the more flexible basis set, 6-311++G(3df,-3pd), using the QCISD and MPW1K optimized geometries. On the basis of initial information, the rate constant for each reaction channel is calculated using the improved canonical variational transition-state theory (ICVT).[16] The $^2P_{1/2}$ and $^2P_{3/2}$ electronic states of the fluorine atom, with a 404 cm^{-1} splitting due to the spin−orbit coupling, are used in the calculation of the electronic partition functions. Finally, the total rate constant is obtained from the sum of the individual rate constant.

Results and Discussion

1. Stationary Points. The geometric parameters of all the stationary points (reactants, complexes, transition states, and products) optimized at the MPW1K/6-311G(d,p) and QCISD/6-311G(d,p) levels are given in Figure 1 together with the available experimental values.[17−22] The geometries of the reactants and products are in reasonable agreement with the experimental values to within the maximum errors of 1% and 4% at the MPW1K and QCISD levels, respectively. For hydrogen abstraction channel R1a (or R2a), there are two hydrogen-bonded complexes CR_{1a} (CR_{2a}) and CP_{1a} (CP_{2a}) located at the reactant and product sides, respectively, in which hydrogen bonds are formed between F atom and H atom of HOCl and between H atom of HF and O atom of ClO, with the H−F and H−O bond distances being 2.25 and 1.85 Å, respectively, and other bond distances are similar to those of the reactant (HOCl) or the products (HF and ClO). The other two complexes (CR_{2a} and CP_{2a}) present the similar description. While for the halogen abstraction channels (R1b and R2b), only one complex is found at the entrance in reaction R2b. In the transition state structures of two hydrogen abstraction reactions, i.e., TS1a and TS2a, the breaking bonds H−O are both elongated by 4% compared to the H−O regular bond lengths in isolated HOCl and HOBr at the MPW1K level; and the forming bonds H−F are both stretched by 53% with respect to the equilibrium bond lengths of the molecule HF. The elongation of the forming bond is greater than that of the breaking bond, indicating that both transition states are reactant-like. On the contrary, two transition states (TS1b and TS2b) of halogen abstraction reactions (R1b and R2b) are product-like, since the stretching of the breaking bond (14 and 13%) is greater than that of the forming bond (7 and 3%). The similar character can be concluded from the geometrical structures optimized at the QCISD/6-311G(d,p) level.

The harmonic vibrational frequencies are calculated at the above two levels to characterize the nature of each critical point and make zero-point energy (ZPE) corrections. The harmonic vibrational frequencies of all the stationary points along with the available experimental data[17,19,23−27] are shown in Table 1. The frequencies are in good accordance with the available experimental values with the maximum error within 9.7% at MPW1K level. And most of the values obtained at the QCISD/6-311G(d,p) level match well with the experimental results except that for the product radical BrO. The QCISD frequency of BrO is 655 cm^{-1}, which slightly underestimates the experimental one, 779 cm^{-1}.[27] The complexes, which are located at the entrance or exit channels, have all real frequencies. All of the transition states are confirmed by normal-mode analysis to have one and only one imaginary frequency, which take the values of 1095*i*(TS1a), 1049*i*(TS1b), 1076*i*(TS2a), and 550*i*(TS2b) at the MPW1K level, respectively, and the corresponding values are 1266*i*, 1043*i*, 1203*i*, and 593*i* at QCISD level.

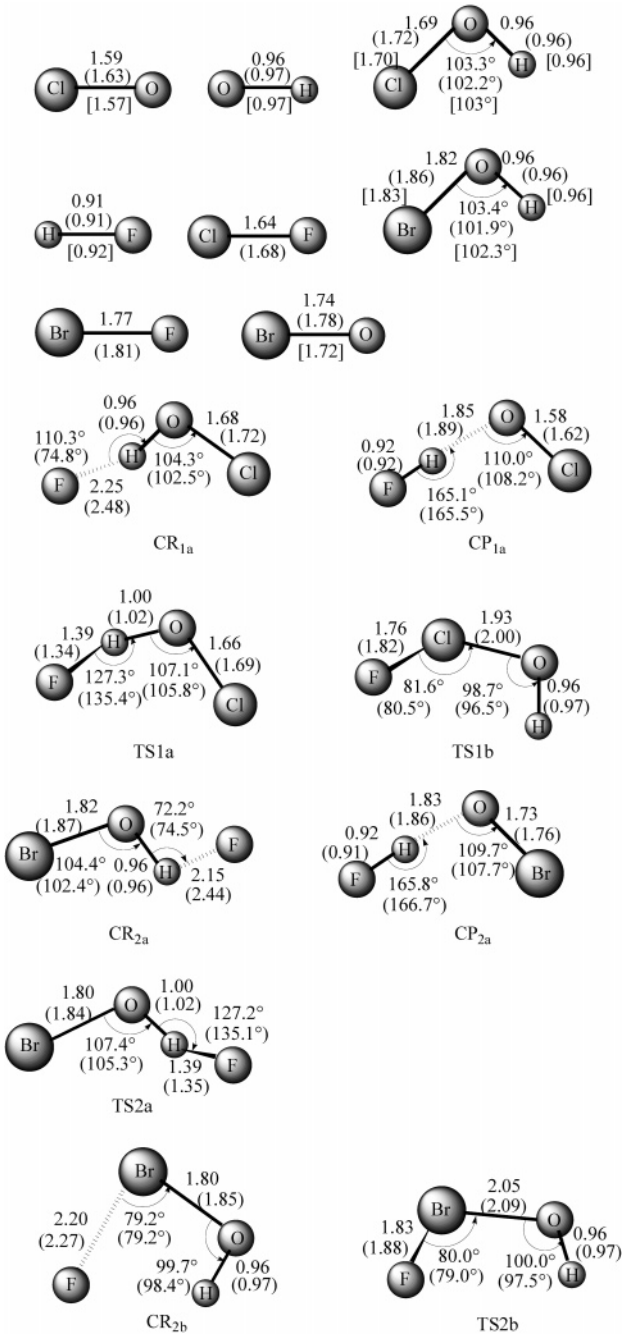

Figure 1. Optimized geometries of HOCl, HOBr, HF, OH, ClO, ClF, BrO, BrF, CR_{1a}, CP_{1a}, CR_{2a}, CP_{2a}, CR_{2b}, and four transition states at the MPW1K/6-311G(d,p) level. The values in parentheses and square brackets are those obtained at the QCISD/6-311G(d,p) level and the experimental values,[17−22] respectively. Bond lengths are in angstroms, and angles are in degrees.

The reaction enthalpies ($\Delta H_{298}°$) of HOCl + F and HOBr + F calculated at several levels are listed in Table 2. The calculated enthalpies for the four reaction channels are −41.21 (R1a), −5.30 (R1b), −38.52 (R2a), and −9.44 (R2b) kcal mol^{-1} at the QCISD(T)//MPW1K level, respectively, and they are −40.48, −5.05, −37.94, and −9.24 kcal mol^{-1} at the QCISD(T)//QCISD level. As can be seen from the four reactions, the enthalpies calculated at the two higher levels agree mutually well. Moreover, the $\Delta H_{298}°$ values of reactions R1a, R1b, and R2a are in good accordance with the experimental values of −41.74 ± 3.3, −4.25 ± 3.1, and −40.14 ± 4.3 kcal mol^{-1}, which are derived from the experimental standard heats of formation (HOCl, −18 ± 3 kcal mol^{-1}; F, 19.0 ± 0.1 kcal

TABLE 1: Calculated and Available Experimental Frequencies (in cm^{-1}) of the Stationary Points at the MPW1K/6-311G(d,p) and QCISD/6-311G(d,p) Levels

	MPW1K/6-311G(d,p)	QCISD/6-311G(d,p)	exptl
HOCl	781, 1285, 3959	702, 1242, 3872	724, 1239, 3609[a]
HF	4309	4250	4138[b]
ClO	848	770	854[c]
OH	3886	3789	3738[d]
ClF	811	721	
HOBr	665,1212, 3965	603, 1183, 3873	620, 1163, 3615[e]
BrO	711	655	779[f]
BrF	704	633	
CR_{1a}	86, 218, 285, 788, 1273, 3936	55, 110, 184, 704, 1236, 3858	
CP_{1a}	60, 204, 419, 583, 877, 4123	59, 192, 437, 585, 792, 4127	
CR_{2a}	72, 228, 297, 671, 1194, 3948	51, 123, 206, 603, 1173, 3860	
CP_{2a}	53, 209, 450, 604, 733, 4089	51, 199, 471, 611, 673, 4096	
CR_{2b}	224, 277, 357, 674, 1265, 3817	203, 210, 327, 595, 1239, 3766	
Ts1a	1095*i*, 146, 328, 808, 1233, 2797	1266*i*, 142, 305, 733, 1231, 2374	
Ts1b	1049*i*, 190, 364, 519, 1046, 3909	1043*i*, 134, 335, 501, 1003, 3799	
TS2a	1076*i*, 122, 325, 681, 1166, 2833	1203*i*, 122, 315, 613, 1184, 2439	
TS2b	550*i*, 176, 314, 552, 982, 3917	593*i*, 159, 306, 517, 961, 3803	

[a] From ref 23. [b] From ref 24. [c] From ref 19. [d] From ref 17. [e] From refs 25 and 26. [f] From ref 27.

TABLE 2: Enthalpies (in kcal mol^{-1}) Calculated at Various Levels and Available Experimental Values

levels	HOCl + F → HF + ClO	HOCl + F → ClF + OH	HOBr + F → HF + BrO	HOBr + F → BrF + OH
MPW1K	−31.66	0.30	−29.46	−4.54
QCISD(T)//MPW1K	−41.21	−5.30	−38.52	−9.44
QCISD	−32.65	−0.59	−31.12	−4.93
QCISD(T)//QCISD	−40.48	−5.05	−37.94	−9.24
exptl[a]	−41.74 ± 3.3	−4.25 ± 3.1	−40.14 ± 4.3	

[a] From refs 17 and 28.

mol^{-1}; OH, 8.85 kcal mol^{-1}; ClF, −12.1 kcal mol^{-1} ClO 24.4 kcal mol^{-1}; HF, −65.14 ± 0.2 kcal mol^{-1}; HOBr, −14 ± 2 kcal mol^{-1}; BrO, 30 ± 2 kcal mol^{-1}).[17,28] Due to lack of the experimental heats of formation for BrF species, it is difficult to make a direct comparison between theory and experiment for the enthalpy of reaction R2b. However, in view of the good agreement obtained above for other three reactions, it is expected that the calculated enthalpies of reaction R2b are reliable.

A schematic potential energy surface of the title reactions with zero-point energy (ZPE) corrections is plotted in Figure 2, parts a and b. Note that the energy of reactant R is set to zero as a reference. For hydrogen abstraction channel F + HOCl → HF + ClO (R1a) or F + HOBr → HF + BrO (R2a), complex CR_{1a} or CR_{2a} with the relative energy −2.28 or −2.59 kcal mol^{-1} at the QCISD(T)//MPW1K level is first formed, then followed by a reactant-like transition state to form the other complex CP_{1a} or CP_{2a}, which is about 4.12 or 4.82 kcal mol^{-1} more stable than the products HF + ClO or HF + BrO. As to the halogen abstraction channels (R1b and R2b), only one well is found at the reactant side of the reaction F + HOBr → OH + BrF (R2b). For two channels of the reaction F + HOCl, the potential barrier heights are −0.60 and 22.55 kcal mol^{-1} at the lower MPW1K level, respectively; even at the higher QCISD-(T)/6-311++G(3df,3pd) single-point level, the barrier height of the Cl-abstraction channel is still higher than that of the H-abstraction channel nearly 12 kcal mol^{-1}, which indicates that the H-abstraction channel (R1a) will dominant the reaction F + HOCl over the entire temperature range and the Cl-abstraction channel will be negligible. As for the reaction F + HOBr (R2), the calculated potential energy surface is different between two levels. It can be seen from Figure 2b that at the MPW1K level the barrier height of the H-abstraction channel (R2a) is lower than that of the Br-abstraction channel (R2b) with values of −0.95 and 6.42 kcal mol^{-1}, respectively. This is similar to the potential energy surface of reaction R1. While the energies of two saddle points are −1.36 for R2a and −3.28 kcal mol^{-1} for R2b relative to the reactants at the QCISD(T)//MPW1K level, implying that the Br-abstraction channel may have important contribution to the whole rate constant. In addition, at the QCISD(T)//QCISD level, the barrier heights of TS1a, TS1b, TS2a, and TS2b are −1.43, 12.77, 0.38, and −2.30 kcal mol^{-1}. It can be found that the results obtained from the two higher levels agree well mutually, i.e., H-abstraction will be the major channel for reaction R1 and Br-abstraction may play an important role for reaction R2. On the basis of the above calculations, we find that the MPW1K method with much less computational expense is available and reliable compared with the QCISD method, which is very expensive. Thus, in the present study, we employ the QCISD(T)//MPW1K method to refine the potential energy surface and calculate the rate constants.

2. Dynamics Calculations. Figure 3 depicts the classical potential energy curve ($V_{MEP}(s)$), the vibrationally adiabatic ground-state potential energy curve ($V_a^G(s)$), and the zero-point energy (ZPE) curve for channel R1a as a function of the intrinsic reaction coordinate *s*. Note that the maximum of the potential energy profile at the QCISD(T)//MPW1K level is slightly shifted in the *s* direction in Figure 3. The similar feature can be drawn for other three reaction channels.

The PES information for each reaction obtained at the QCISD(T)/6-311++G(3df,3pd)//MPW1K/6-311G(d,p) level is put into the Polyrate 8.4.1 program[11] to calculate the VTST[12−14] rate constants over the temperature range from 200 to 2000 K. The rate constants for each reaction channel are calculated by the conventional transition state theory (TST) and the improved canonical variational transition-state theory (ICVT).[16] The total rate constants for the title reaction are obtained from the sum of the individual rate constants associated with the two channels. Note that it is found that although for all the reactions the dynamical bottleneck actually do not occur at the saddle point, the locations are very close to the saddle point, with the most furthest shift about $0.1(amu)^{1/2}$ bohr at the QCISD(T)//MPW1K

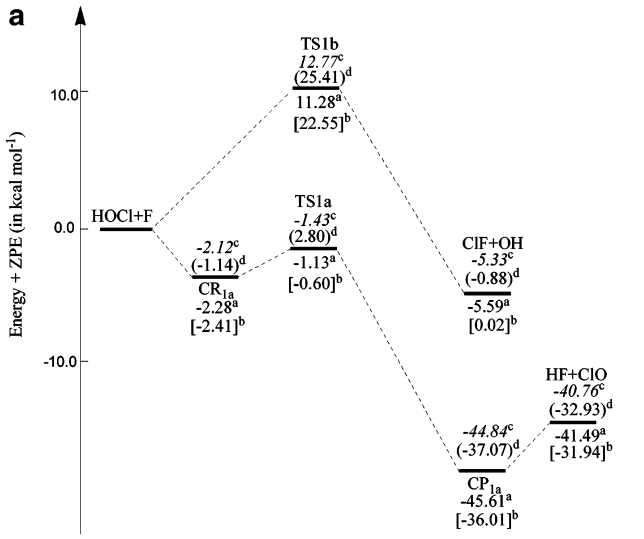

[a]Calculated at the QCISD(T)/6-311++G(3df, 3pd)//MPW1K/6-311G(d, p) level
[b]Calculated at the MPW1K/6-311G(d, p) level
[c]Calculated at the QCISD(T)/6-311++G(3df, 3pd)//QCISD/6-311G(d, p) level
[d]Calculated at the QCISD/6-311G(d, p) level

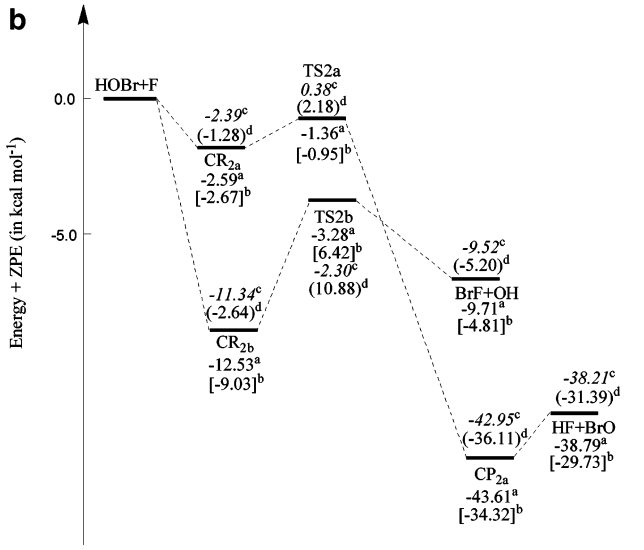

[a]Calculated at the QCISD(T)/6-311++G(3df, 3pd)//MPW1K/6-311G(d, p) level
[b]Calculated at the MPW1K/6-311G(d, p) level
[c]Calculated at the QCISD(T)/6-311++G(3df, 3pd)//QCISD/6-311G(d, p) level
[d]Calculated at the QCISD/6-311G(d, p) level

Figure 2. Schematic pathways for the reactions (a) F + HOCl and (b) F + HOBr.

level. Thus, it is reasonable to calculate the rate constant using the variational transition state theory.

The temperature dependence of thebranching ratios k_{1a}/k_1, k_{1b}/k_1, k_{2a}/k_2, and k_{2b}/k_2 is exhibited in Figure 4, parts a and b. From Figure 4a, we find that chloride abstraction channel is negligible due to the higher barrier height, while the hydrogen abstraction is the predominant or exclusive channel for reaction F + HOCl over the whole temperature range with the ratio of k_{1a}/k_1 close to unity. The H-abstraction mechanism we obtain is in accord with the experimental result reported by Vogt and Schindler,[5] although there is some discrepancy between the calculated and experimental branching ratio (1.0 vs 76 ± 9 %). With respect to the reaction of F + HOBr, Mook et al.[6] assumed that the major products are BrO and HF by analogy with the result for F + HOCl. However, up to now, no further experiment has

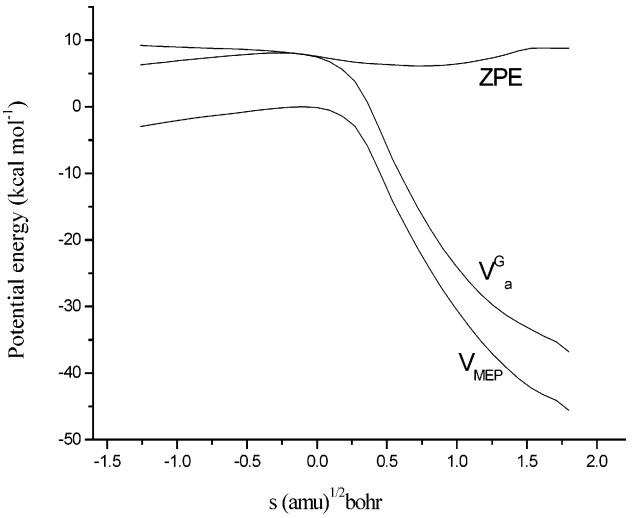

Figure 3. Classical potential energy curve (V_{MEP}), ground-state vibrationally adiabatic energy curve (V_a^G), and zero-point energy curve (ZPE) as functions of s (amu)$^{1/2}$ bohr at the QCISD(T)/6-311++G-(3df,3pd)//MPW1K/6-311G(d,p) level for the F + HOCl → HF + ClO.

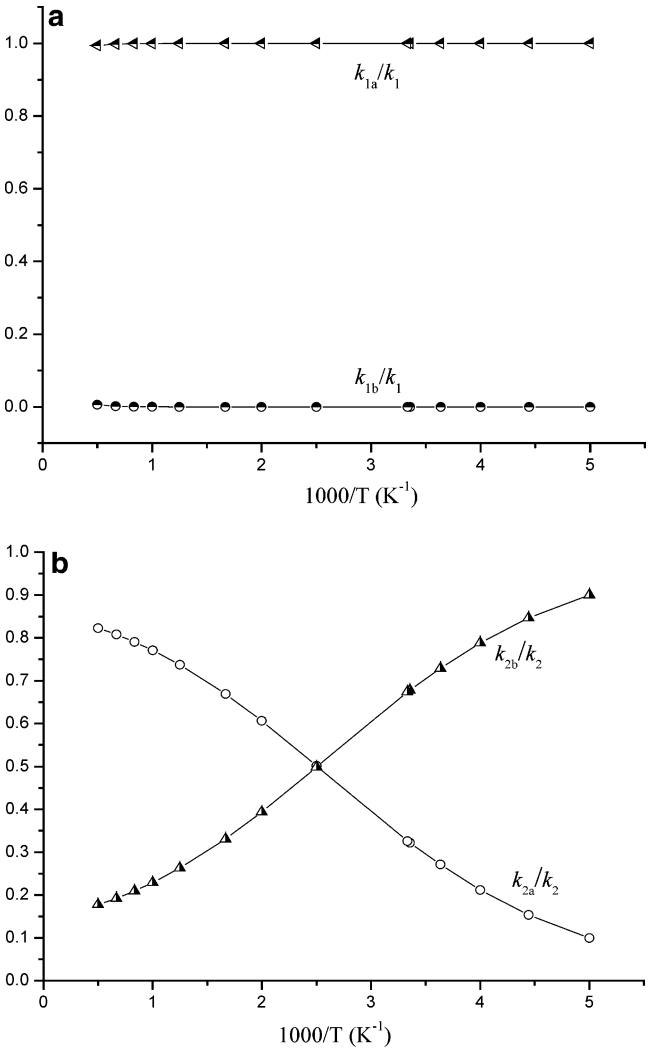

Figure 4. Plot of the calculated branching ratio vs 1000/T between 200 and 2000 K for the (a) F + HOCl and (b) F + HOBr.

been done to determine the ratio of the reaction F + HOBr. It is seen from Figure 4b that the Br-abstraction leading to the product BrF + OH dominants the reaction at the lower temperature, while the contribution of H-abstraction prevails

TABLE 3: Rate Constants (in cm^3 molecule^{-1} s^{-1}) for the Reaction HOX + F (X = Cl or Br) in the Temperature Range 200−2000 K

(a) HOCl + F[a]

T (K)	k_{1a}	k_{1b}	k_1	exptl
200	5.11×10^{-11}	3.54×10^{-25}	5.11×10^{-11}	
225	4.64×10^{-11}	9.10×10^{-24}	4.64×10^{-11}	
250	4.35×10^{-11}	1.24×10^{-22}	4.35×10^{-11}	
275	4.17×10^{-11}	1.06×10^{-21}	4.17×10^{-11}	
298	4.06×10^{-11}	5.58×10^{-21}	4.06×10^{-11}	$(4.9 \pm 0.6) \times 10^{-11}$ [b]
300	4.05×10^{-11}	6.38×10^{-21}	4.05×10^{-11}	
400	3.91×10^{-11}	9.56×10^{-19}	3.91×10^{-11}	
500	4.04×10^{-11}	2.08×10^{-17}	4.04×10^{-11}	
600	4.30×10^{-11}	1.71×10^{-16}	4.30×10^{-11}	
800	5.02×10^{-11}	2.61×10^{-15}	5.02×10^{-11}	
1000	5.88×10^{-11}	1.45×10^{-14}	5.88×10^{-11}	
1200	6.82×10^{-11}	4.78×10^{-14}	6.82×10^{-11}	
1500	8.32×10^{-11}	1.68×10^{-13}	8.34×10^{-11}	
2000	1.10×10^{-10}	6.54×10^{-13}	1.11×10^{-10}	

HOBr + F[c]

T (K)	k_{2a}	k_{2b}	k_2	exptl
200	9.71×10^{-11}	8.80×10^{-10}	9.77×10^{-10}	
225	8.03×10^{-11}	4.44×10^{-10}	5.24×10^{-10}	
250	6.98×10^{-11}	2.60×10^{-10}	3.30×10^{-10}	
275	6.28×10^{-11}	1.69×10^{-10}	2.31×10^{-10}	
298	5.83×10^{-11}	1.23×10^{-10}	1.81×10^{-10}	$(2.0 \pm 0.7) \times 10^{-10}$ [d]
300	5.80×10^{-11}	1.20×10^{-10}	1.78×10^{-10}	
400	4.93×10^{-11}	4.90×10^{-11}	9.83×10^{-11}	
500	4.75×10^{-11}	3.08×10^{-11}	7.83×10^{-11}	
600	4.82×10^{-11}	2.38×10^{-11}	7.20×10^{-11}	
800	5.27×10^{-11}	1.88×10^{-11}	7.15×10^{-11}	
1000	5.93×10^{-11}	1.76×10^{-11}	7.69×10^{-11}	
1200	6.68×10^{-11}	1.77×10^{-11}	8.45×10^{-11}	
1500	7.94×10^{-11}	1.89×10^{-11}	9.83×10^{-10}	
2000	1.03×10^{-10}	2.22×10^{-11}	1.25×10^{-10}	

[a] k_{1a} and k_{1b} represent the ICVT rate constants of reactions R1a, R1b, and k_1 represents the total rate constant $R1$ calculated from the sum of two ICVT rate constants. [b] From ref 5. [c] k_{2a} and k_{2b} represent the ICVT rate constants of reactions R2a, R2b, and k_2 represents the total rate constant $R2$ calculated from the sum of two ICVT rate constants. [d] From ref 6.

over the Br-abstraction and becomes more important above 400 K. For example, the k_{2a}/k_2 ratios are 11% at 200 K, 50% at 400 K, and 81% at 1500 K. Consequently, the H-abstraction channel becomes the major pathway at higher temperature.

The ICVT rate constants of k_{1a}, k_{1b}, and the total rate constants k_1 along with the available experimental values[5,6] are listed in Table 3a and Figure 5a. It can be found that at the room temperature the calculated rate constant (k_1) is in good agreement with the experimental value[5] $(4.9 \pm 0.6) \times 10^{-11}$ cm^3 molecule^{-1} s^{-1}. Similar conclusion can be drawn for reaction R2 from Table 3b and Figure 5b. At room temperature the calculated rate constant agrees well with the value reported by Mooks et al.[6]

Finally, to provide estimate for the kinetics of the reactions in other temperatures where no experimental values are available, the three-parameter fits for the ICVT rate constants for the title reactions within 200−2000 K give the following expressions (in cm^3 molecule^{-1} s^{-1}):

$$k_1 = 4.32 \times 10^{-11} T^{-0.12} \exp(172.4/T)$$

$$k_2 = 3.31 \times 10^{-17} T^{1.91} \exp(1395.7/T)$$

Conclusion

In this paper, we employ density functional theory and ab initio direct dynamic method to study the reactions of F + HOX (X = Cl and Br). The rate constant calculations are carried out using the variational transition-state theory (VTST) at the QCISD(T)/6-311++G(3df,3pd)//MPW1K/6-311G(d,p) level over a wide temperature range of 200−2000 K. The total rate constants of the title reactions agree well with the available experimental values. It is shown that for the F + HOCl reaction, the reaction occurs exclusively via the hydrogen abstraction, while both hydrogen and bromine abstractions are involved in the F + HOBr reaction, and the hydrogen abstraction is preferred when the temperature is higher than 400 K. The three-parameter expressions (in cm^3 molecule^{-1} s^{-1}) for the title reactions within 200−2000 K are $k_1 = 4.32 \times 10^{-11} T^{-0.12} \exp(172.4/T)$ and $k_2 = 3.31 \times 10^{-17} T^{1.91} \exp(1395.7/T)$.

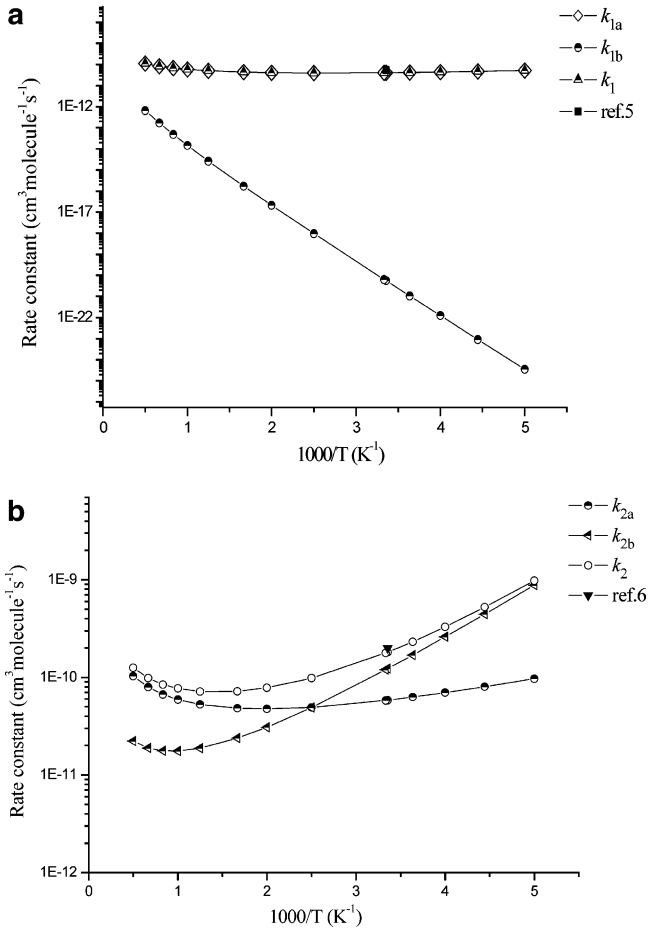

Figure 5. Plot of the ICVT rate constants calculated at the QCISD-(T)/6-311++G(3df,3pd)//MPW1K/6-311G(d,p) level and the available experimental valuesversus 1000/T between 200 and 2000 K for the (a) F + HOCl and (b) F + HOBr.

Acknowledgment. We thank Professor Donald G. Truhlar for providing of the POLYRATE 8.4.1 program. This work was supported by the National Natural Science Foundation of China (20333050, 20303007, 20073014), the Doctor Foundation by the Ministry of Education, the Foundation for University Key Teacher by the Ministry of Education, the Key Subject of Science and Technology by the Ministry of Education of China, and the Innovational Foundation by Jilin University.

References and Notes

(1) Scientific Assessment of Ozone Depletion, 1994; WMO Global Ozone Research Monitoring Project, Report 37, 1995.

(2) Yung, Y. L.; Pinto, J. P.; Watson, R. T.; Sander, S. P. *J. Atmos. Sci.* **1980**, *37*, 339.

(3) Poulet, G.; Pirre, M.; Maguin, F.; Ramaroson, R.; LeBras, G. *Geophys. Res. Lett.* **1992**, *19*, 2305.

(4) Garcia, R. R.; Solomon, S. J. *Geophys. Res.* **1994**, *99*, 937.

(5) Vogt, R.; Schindler, R. N. *Ber. Bunsen-Ges. Phys. Chem.* **1993**, *97*, 819.

(6) Mooks, P. S.; Nesbitt, F. L.; Scanlon, M.; Stief, L. J. *J. Phys. Chem.* **1993**, *97*, 11699.

(7) Wang, L.; Liu, J. Y.; Li, Z. S.; Huang, X. R.; Sun, C. C. *J. Phys. Chem.* **2003**, *107*, 4921.

(8) Truhlar, D. G. In *The reaction Path in Chemistry: Current Approaches and Perspectives*; Heidrich, D., Ed.; Kluwer: Dordrecht, The Netherlands, 1995; p 229.

(9) Truhlar, D. G.; Garrent, B. C.; Klippenstein, S. J. *J. Phys. Chem.* **1996**, *100*, 12771.

(10) Hu, W. P.; Truhlar, D. G. *J. Am. Chem. Soc.* **1996**, *118*, 860.

(11) Chuang, Y.-Y.; Corchado, J. C.; Fast, P. L.; Villa, J.; Hu, W.-P.; liu, Y. −P.; Lynch, G. C.; Jackels, C. F.; Nguyen, K. A.; Gu, M. Z.; Rossi, I.; Coitino, E. L.; Clayton, S.; Melissas, V. S.; Lynch, B. J.; Steckler, R.; Garrett, B. C.; Isaacson, A. D.; Truhlar, D. G. *Polyrate version 8.4.1*; University of Minnnesota: Minneapolis, MN, 2000.

(12) Truhlar, D. G.; Garrett, B. C. *Acc. Chem. Res.* **1980**, *13*, 440.

(13) Truhlar, D. G.; Isaacson, A. D.; Garrett, B. C. In *The Theory of Chemical Reaction Dynamics*; Baer, M., Ed.; CRC Press: Boca Raton, FL, 1985, p 65.

(14) Truhlar, D. G.; Garrett, B. C. *Annu. Rev. Phys. Chem.* **1984**, *35*, 159.

(15) GAUSSIAN 98, Revision A.7, Frisch, M. J.; Trucks, G. W.; Schlegel, H. B.; et al.; Gaussian, Inc.: Pittsburgh, PA, 1998.

(16) Garrett, B. C.; Truhlar, D. G.; Grev, R. S.; Magnuson, A. W. *J. Phys. Chem.* **1980**, *84*, 1730.

(17) Chase, M. W.; Jr. *J. Phys. Chem. Ref. Data* **1998**, Monograph 9, 1−1951 (NIST-JANAF Themochemical Tables, 4th ed.).

(18) Kuchitus, K. *Structure of Free Polyatomic Molecules Basic Data*; 1998; Vol. 1, p 35.

(19) Distelrath, V.; Boesl, U. *Faraday. Discuss. Chem. Soc.* **2000**, *115*, 161.

(20) Amano, T.; Yoshinaga, A.; Hirota, E. *J. Mol. Spectrosc.* **1972**, *44*, 594.

(21) Koga, Y.; Taleo, H.; Londo, S.; Sugie, M.; Matsumura, C.; Mcrae, G. A.; Cohen, E. A. *J. Mol. Struct.* **1989**, *138*, 467.

(22) Fishburne, E. S.; Rao, K. N. *J. Mol. Spectrosc.* **1966**, *19*, 290.

(23) Junttila, M.-L.; Lafferty, W. J.; Burkholder, J. B. *J. Mol. Spectrosc.* **1994**, *164*, 583.

(24) Webb, D. U.; Rao, K. N. *J. Mol. Spectrosc.* **1968**, *28*, 121.

(25) Barnes, I.; Bastian, V.; Becker, K. H.; Overath, R.; Zhu, T. *Int. J. Chem. Kinet.* **1989**, *21*, 499.

(26) Mcrae, G. A.; Cohen, E. A. *J. Mol. Spectrosc.* **1990**, *139*, 369.

(27) Durie, R. A.; Ramsay, D. A. *Can. J. Phys.* **1958**, *36*, 35.

(28) (a) Ruscic, B.; Feller, D.; Dixon, D. A.; Peterson, K. A.; Harding, L. B.; Asher, R. L.; Wagner, A. F. *J. Phys. Chem. A* **2001**, *105*, 1. (b) Joens, J. A. *J. Phys. Chem. A* **2001**, *105*, 11041. (c) Ruscic, B.; Wagner, A. F.; Harding, L. B.; Asher, R. L.; Feller, D.; Dixon, D. A.; Peterson, K. A.; Song, Y.; Qian, X.; Ng, C. Y.; Liu, J.; Chen, W.; Schwenke, D. W. *J. Phys. Chem. A* **2002**, *106*, 2727.